

[Click here to view linked References](#)

Multi-technique diagnostic analysis and 3D surveying prior the restoration of *St. Michael defeating Evil* painting by Mattia Preti

Sebastiano D'Amico^{1,†}, Valeria Comite^{2,†}, Giuseppe Paladini^{3,*}, Michela Ricca^{4,*}, Emanuele Colica¹, Luciano Galone¹, Sante Guido⁵, Giuseppe Mantella⁶, Vincenza Crupi⁷, Domenico Majolino³, Paola Fermo², Mauro Francesco La Russa⁴, Luciana Randazzo⁴, Valentina Venuti³

¹Department of Geosciences, University of Malta, Msida Campus, MSD 2080, Malta

²Department of Chemistry, University of Milan, Via Golgi 19, 20133, Milan, Italy

³Department of Mathematical and Computer Sciences, Physical Sciences and Earth Sciences, University of Messina, Viale Ferdinando Stagno D'Alcontres 31, I-98166 Messina, Italy

⁴Department of Biology, Ecology and Earth Sciences, University of Calabria, 87036 Arcavacata di Rende (CS), Italy

⁵Department of Literature and Philosophy, University of Trento, Via Tommaso Gar, 14, I-38122 Trento, Italy

⁶Giuseppe Mantella Restauro Opere D'Arte, Circonvallazione Paparo 25, Isca sullo Ionio, (CZ) 88060, Italy

⁷Department of Chemical, Biological, Pharmaceutical and Environmental Sciences, University of Messina, Viale Ferdinando Stagno D'Alcontres 31, I-98166 Messina, Italy

[†]These Authors contributed equally to this study

*Corresponding author e-mail: gpaladini@unime.it, michela.ricca@unical.it

Abstract

In this study, a multi-methodological analysis involving optical and physical/chemical diagnostic techniques and 3D photogrammetric survey was successfully applied, for the first time, on the large *St. Michael defeating Evil* painting by Mattia Preti, located inside the Church of the Immaculate Conception of Sarria (Floriana) in Malta. Pigmenting agents, binder media and raw materials were first characterized, both at elemental and molecular scales, through X-ray fluorescence spectroscopy (XRF), optical stereo microscopy (SM), scanning electron microscopy coupled with energy dispersive X-ray spectroscopy (SEM-EDX), Fourier transform infrared spectroscopy (FT-IR) and gas chromatography coupled with mass spectrometry (GC-MS). The main goal was to properly identify the execution technique of this famous painter, the pigment's palette and possible non-documented interventions. The 3D photogrammetric survey, on the other side, allowed us to non-invasively evaluate the extension of the areas that experienced restorations, and to properly map the domains of the different canvases observed. The joints between canvases suggested that the painting was folded and rolled up. In addition, the employment of a thermal camera gave evidence of the different consolidating material injection points used during the restoration to strengthen the painting. The obtained results offer useful information for the development of optimized restoration and conservation strategies to be applied and provide, at the same time, answers to open questions related to provenance and dating of the investigated artwork.

Keywords

Conservation, Lunette, Mattia Preti, Pigment's identification, Globigerina limestone, Multi-technique analysis, 3D photogrammetric survey

1. Introduction

57 The *St. Michael defeating Evil* painting is a masterpiece of the painter Mattia Preti, a renowned Italian artist
58 active in Malta between 1661 and 1699, the year of his death. It is one of the seven paintings that Mattia Preti
59 executed inside the Church of the Immaculate Conception of Sarria (Fig. 1a-c) in Floriana (Malta), in occasion
60 of its reconstruction in 1677 as *ex voto* for the end of the plague in 1676. The Church, commissioned by the
61 Grand Master of the Knights of Malta, friar Nicolas Cottner, is characterized by a central plan almost totally
62 designed by Mattia Preti himself. The pictorial cycle includes five paintings depicting *Mary Immaculate and the*
63 *Saints protectors from the plague* and, painted on two large Lunettes, two examples of the *struggle of Good*
64 *against Evil* in relation to the plague disease interpreted as divine punishment. These “oil on canvas” paintings
65 were all executed between 1677 and 1679, and are essentially inspired by subjects that Mattia Preti had depicted
66 almost twenty years earlier in seven frescoes, on as many gates of the city of Naples, as *ex voto* for the end of
67 the plague epidemic of 1656.

68 The *St. Michael defeating Evil* painting, under investigation in the present study, is one of the two Lunettes
69 of the arches (see Fig. 1d), together with the *Allegory of the Order of St. John the Baptist* painting (Fig. 1e). This
70 large-sized (235 cm × 475 cm) work depicts the exterminating Archangel dressed as a Knight of the Order of
71 Malta, with armor and bright red cloak, as he bursts from above holding his sword at the head of a host of
72 executioner angels armed with foils and lightning bolts, ready to punish demons, offenders and sinners depicted
73 in a tangle of lifeless bodies or dismayed and subjugated by terror.

74 At the beginning of the restoration process, the painting appeared seriously damaged, being the canvas
75 heavily compromised and the pictorial surface severely re-painted and darkened by oils and waxes applied over
76 the years. Therefore, it was necessary to study the dramatic state of conservation of the painting thanks to
77 archival research, in order to understand the problems of the work and to plan the most appropriate scientific
78 investigations to be executed.

79 In particular, it was understood that over the centuries the Lunette had undergone several conservation
80 interventions, two of which documented by archival sources.

81 In the 30s of the twentieth century, considering the poor conservation conditions (the painting must already
82 have been very incomplete) it was reupholstered on a new canvas.

83 The work was the subject of a very bad lining operation which involved the almost complete detachment of
84 the original canvas and the application of only the preparation and the pictorial film on a new canvas. The gluing
85 was performed with animal glue, not very elastic, which in a few years, due to a polymerization process, stiffened
86 the painting to completion. During this operation, the numerous gaps created were filled with plaster and glue
87 colored with iron oxide, in order to match them chromatically with the original brown-colored preparation by
88 Mattia Preti. By means of oil colors, the gaps created with the detachment of large portions were completely
89 repainted, and many of the original figures that were lost were re-proposed.

90 Concerning the second documented intervention, it took place after the Second World War. At that time, the
91 most important paintings in churches throughout the island of Malta were protected at the outbreak of the conflict
92 by collecting and hiding them in bunkers in uninhabited areas. In particular, in the case of the *St. Michael*
93 *defeating Evil* painting, the artwork was removed from the frame and rolled up. The latter operation caused very
94 serious damages, due to the stiffening of the glue employed in the 30s, which caused the tearing of the artwork
95 into overlapping bands. In the 50s, a new conservative intervention was carried out, during which, since the re-
96 sheathed canvas could not be removed, a new canvas was applied over the previous one, this time with paste,
97 unfortunately free of bactericide. In addition, new gaps were plastered and some new re-paintings were carried
98 out.

99 In the framework of restoration interventions, the possibility to create digital models and 3D replicates of
100 objects/artworks of historical and artistic value has gained, in recent years, considerable attention (Yilmaz et al.
101 2007; Arias et al. 2007; Armesto et al. 2008; Remondino et al. 2009; Remondino 2011; Fiorillo et al. 2015;
102 Balletti et al. 2016; Aicardi et al. 2018; D’Amico et al. 2020). As a matter of fact, digitization of artifacts by
103 triangulation procedures allows the assembly of digital archives which can be used to plan and support the
104 different restoration phases. In addition, 3D reconstructions are quite simple to be accomplished, providing at
105 the same time reliable information about the spatial/geometrical properties of objects and environments,
106 basically without any direct contact. To further support the definition of optimized restoration and conservation
107 strategies to be applied to artifacts, the multi-technique characterization, through complementary, non- or at least
108 micro-destructive methodologies, of the constituent materials such as pigmenting agents, binding media and
109 preparatory materials, represents an extremely valuable source of information (Edwards et al. 2004; Castro
110 et al. 2008; Bersani et al. 2008, 2014; Rosi et al. 2009; Tschegg et al. 2009; Ruffolo et al. 2010; Barbera et al.
111 2012; La Russa et al. 2014; Comite and Ricca 2016; Crupi et al. 2018; Ricca et al. 2019; Venuti et al. 2020;
112 Zueno et al. 2020; Fermo et al. 2020) in order to give answers concerning open problems such as execution
113 technique, dating and provenance.

114 In this work, a preliminary *in-situ* investigation through portable X-ray fluorescence spectroscopy (XRF)
115 allowed for the identification, at the elemental scale, of the composition of some representative areas, in terms
116 of major and minor constituents. Then, a sampling procedure was performed in order to assess the samples

117 stratigraphy, and to better understand the pigment's palette and the raw materials used by the artist for the
118 preparatory layer and for the painting, by applying optical stereo microscopy (SM) and scanning electron
119 microscopy coupled with energy dispersive X-ray spectroscopy (SEM-EDX). In addition, Fourier transform
120 infrared spectroscopy (FT-IR) was adopted to primarily identify inorganic compounds although the technique,
121 in the field of Cultural Heritage, is mainly used for the identification of the organic ones. In the specific case,
122 investigations were carried out to characterize the superficial and painted layers of the samples and to further
123 support the investigations conducted by XRF and SEM-EDX. Moreover, gas chromatography coupled with mass
124 spectrometry (GC-MS) was used for a preliminary investigation of the used binders.

125 Along with a detailed diagnostic investigation of the materials composition, the 3D digitalization of the
126 masterpiece allowed us to highlight, for the first time on a painting by Mattia Preti, the unevenness of the original
127 surfaces as well as the presence of layers subsequently applied during the various restoration interventions.

128 It is worth underlying that the knowledge of all the aforementioned aspects does not simply constitute a
129 fundamental pre-requisite in view of the development of proper restoration strategies to be applied. As a matter
130 of fact, being the composition of the grounds of Italian painters of the 17th century, such as Mattia Preti,
131 connected to the place where the artwork was realized (Hradil et al. 2020), the identification of the source
132 materials represents the groundwork for dating and locating the *St. Michael defeating Evil* painting to a specific
133 period of the artist's productive life, i.e. in Italy or in Malta. This is, at present, an ongoing controversy among
134 the scientific community, also considering the close relation between these two regions.

135



136

137

138 **Fig. 1** a) Map of Malta, with the town of Floriana indicated. b) External and c) internal view of the Church of the
139 Immaculate Conception of Sarria in Floriana, Malta. d) *St. Michael defeating Evil* and e) the *Allegory of the Order*
140 *of St. John the Baptist* paintings

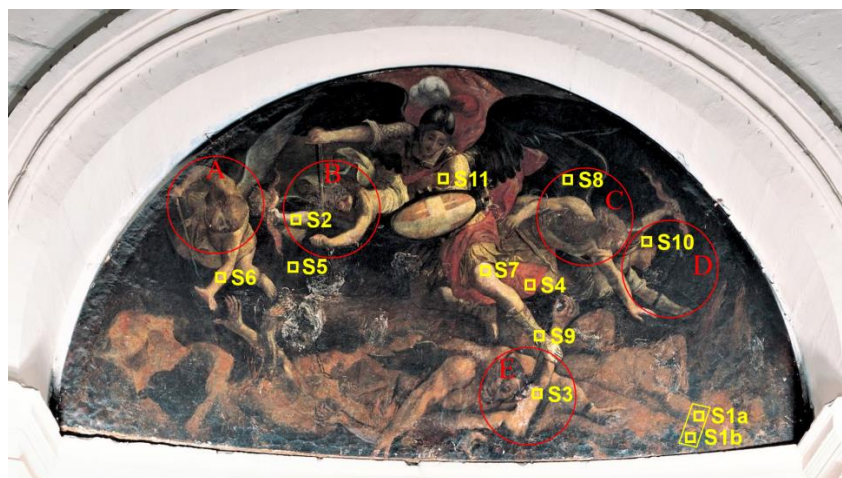
141

142 2. Materials and methods

143

144 Overall, 12 points were investigated, *in situ* and in the laboratory (see Fig. 2).

145



146
147
148
149
150
151
152
153
154
155
156
157
158

Fig. 2 Analyzed points from the *St. Michael defeating Evil* painting. Red circles account for the position of the four angels (A-D) and the devil (E)

In particular, as far as laboratory analyses are concerned, 11 micro-fragments of the pictorial surface (size smaller than $\sim 5 \text{ mm}^2$) were sampled from the edge of already-existing lacunae, in proximity of ageing-induced surface cracks, during the latest restoration intervention in 2019. This allows the characterization of the pictorial technique as well as of overlapping layers on the painting. Details about sampling are described in Table 1, together with all the analytical techniques employed.

Table 1 Investigated samples, description and techniques employed

Sample ID	Description	Techniques employed
S1a ^a	Bottom, right-side of the canvas, <i>Light area</i>	XRF
S1b	Bottom, right-side of the canvas, <i>Dark area</i>	XRF, SM, SEM-EDX, FT-IR
S2	Right arm of the angel on the left (B), <i>Brown-gray</i>	SM, SEM-EDX, FT-IR
S3	Right arm of the devil (E), <i>Uncertain color tending to brownish-bluish</i>	SM, SEM-EDX, FT-IR, CG-MS
S4	Cloak of <i>St. Michael</i> , <i>Red</i>	XRF, SM, SEM-EDX, FT-IR
S5	Angel wing on the left (A), <i>Black</i>	XRF, SM, SEM-EDX, FT-IR
S6	Incarnate of the angel on the left (A), <i>Beige</i>	SM, SEM-EDX, FT-IR
S7	Incarnate of <i>St. Michael</i> , <i>Uncertain color tending to beige-grayish</i>	SM, SEM-EDX, FT-IR, CG-MS
S8	Angel wing on the right (C), <i>Blackish-brownish</i>	XRF, SM, SEM-EDX, FT-IR
S9	Sandalwood of <i>St. Michael</i> , <i>Green-yellowish</i>	XRF, SM, SEM-EDX, FT-IR
S10	Hair of the angel on the right (D), <i>Uncertain color tending to brownish</i>	SM, SEM-EDX, FT-IR
S11	<i>St. Michael's</i> armor, <i>Uncertain color tending to beige-grayish</i>	SM, SEM-EDX, FT-IR

159
160
161

^aUnfortunately, due to practical difficulties, the sampling of micro-fragment S1a was not possible. Accordingly, only *in-situ* XRF spectroscopy was carried out.

162 It is worth underlying that the sampling procedure was conducted following minimal invasiveness principles,
163 and taking into account that the painting under investigation was, at the time, in an advanced state of deterioration.
164 In this sense, the identification of colors by visual inspection turned out to be a very challenging task.

165 XRF spectra were collected through a portable XRF "Alpha 4000" (Innov-X system) analyzer, which allowed
166 the detection of chemical elements having an atomic number (Z) between phosphorus and lead. The instrument
167 was equipped with a Ta anode X-ray tube excitation source, and a Si PIN diode detector with an active area of
168 170 mm². The apparatus operated using a Compton Normalization algorithm ("soil" mode), designed for
169 achieving the lowest Limit of Detection (LOD) possible (trace concentrations, from levels of ppm) for soil and
170 bulk samples. The "soil" mode was here adopted together with the "Environmental" elements suite. For the used
171 "soil" mode, the following element list was used: P, S, Cl, K, Ca, Ti, Cr, Mn, Fe, Co, Ni, Cu, Zn, As, Se, Br, Rb,
172 Sr, Zr, Mo, Ag, Cd, Sn, Sb, I, Ba, Au, Hg, Pb. For each analysed area, two sequential tests were carried out. In
173 particular, the working conditions were 40 kV and 7 μ A for the first one and, 15 kV and 5 μ A for the second one,
174 for a total collection time of 120 s (60 s per run). A Hewlett-Packard iPAQ Pocket PC was used to manage the
175 instrument and as data storage. The calibration was carried out by soil LEAP (Light Element Analysis Program)
176 II and was verified using alloy certified reference materials produced by Analytical Reference Materials
177 International. Lines detected at \sim 8.15 keV and \sim 9.34 keV, observed for all the investigated samples, were
178 attributed to the L _{α} and L _{β} energy transition of Ta anode.

179 Stereomicroscopic investigations were conducted to closely examine the cross sections of the samples and
180 were carried with a Zeiss Axiolab microscope equipped with a digital camera to capture images. Observations
181 allowed to highlight the different structure of samples, i.e. the stratigraphy and the overlapping of the various and
182 subsequent layers.

183 SEM-EDX analyses were performed on the surface of the samples (both on the back and on the front of the
184 fragments) to obtain information about the micromorphology and chemical composition (in term of major
185 elements). Analyses were performed with a scanning electron microscope Hitachi TM4000, equipped with a
186 detector STEM. Microanalysis was performed using an energy dispersive spectrometry EDX Oxford -AztecOne.
187 Analyses were carried out with an acceleration voltage of 5 kV, 10 kV e 15 kV and under high vacuum conditions.

188 As FT-IR is concerned, the spectrophotometer used was a Perkin Elmer Spectrum 100, equipped with an
189 attenuated total reflectance (ATR) accessory. Infrared spectra were recorded in ATR mode, in the range of 500–
190 4000 cm⁻¹ at a resolution of 4 cm⁻¹. Due to the complexity of the FT-IR absorbance profiles, the samples' spectra
191 were also compared with those of standard minerals and/or pigments from databases (Vahur et al. 2016) and
192 literature (Derrick et al. 2000) for a reliable assignment of the bands.

193 The determination of the organic binding media was carried out by means of gas chromatography/mass (GC-
194 MS) technique using a GC-MS_TQ8040NX instrument (Shimadzu); He was the carrier gas (1mL/min) and
195 separation was achieved by a capillary column VF-5ms (26 m x 0.25 mm i.d. x 0.25 μ m). The sample (1 μ L) was
196 introduced into the column by splittess injection with the following temperature program: 100°C for 2 minutes,
197 6°C/min up to 280°C, and finally 280°C for 10 minutes. Mass spectra were recorded in full-scan mode with the
198 m/z range 50-1000 amu. Sample preparation was achieved following a consolidated procedure reported in the
199 literature (Colombini et al. 1999); briefly the micro-fragment was submitted to a previous clean-up procedure by
200 NH₃ and to an acid hydrolysis by HCl 6M and a subsequent derivatization by BSTFA.

201 Concerning the 3D survey, the final 3D model was obtained (Fig. 3) by applying the processing and workflow
202 described in (Colica et al. 2018) and (D'Amico et al. 2017), and after the fine mesh geometry generation and
203 reconstruction, the model was textured and used also for orthomosaic generation. Finally, a Digital Elevation
204 Model (DEM) of the surface was generated. The same process was applied also to images acquired using ultra-
205 violet (UV) light and a different digital model of the painting was generated (Fig. 3a). An accurate 3D model of
206 the frame was also obtained (Fig. 3b).

207

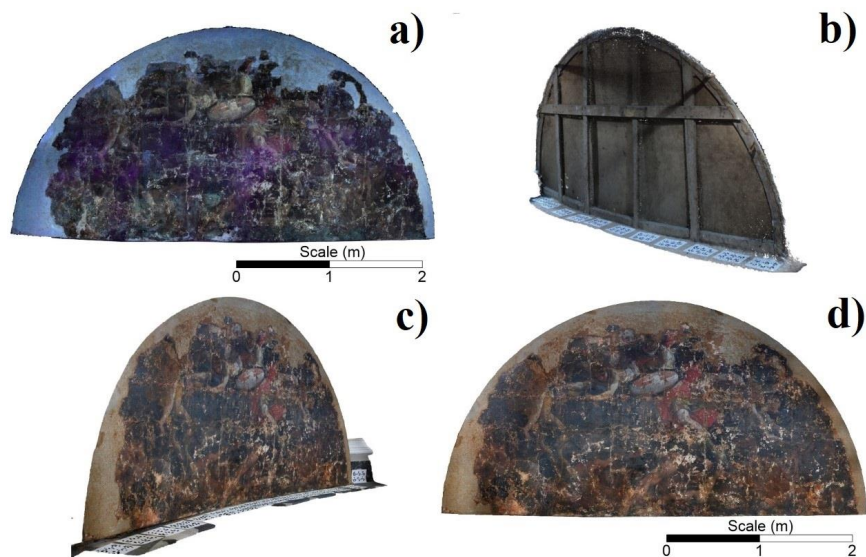


Fig. 3 3D photogrammetric reconstruction of the *St. Michael defeating Evil* painting. **a)** Model reconstructed using the UV light, **b)** 3D model of the painting frame, **c)** and **d)** show the 3D model and the orthophoto obtained using the RGB pictures

Both 3D digital Red-Green-Blue (RGB) (Fig. 3c-d) and UV (Fig. 3a) models were inspected for a first visual analysis and different filters were applied in order to improve the contrast between the different areas and parts of the painting. In particular, the use of the UV orthophoto, coupled with some information gathered during the physical survey, allowed to discriminate regions potentially covered by the original painting or subsequent restorations. To the referenced and measurable 3D RGB model a 3x3 filter was firstly applied, in order to smooth the DEM with the main goal of eliminating noisy points that generate a false rugose texture. After this step, we applied a typical set of procedures that are usually used in topographical analysis. In this context, the high-resolution of the 3D model and the accurate measurements allowed us to use technique not quite often used in archaeometry and mainly used for large scale objects, such as topographic profiles at different scales, contour maps, hill shading visualization and 3D visualization. This approach allowed us to obtain a very good representation of the topographic variations spanning from the millimetric to the metric scale and gave us the possibility to identify topographic alignments as well as mapping other morphologic features. An ad-hoc Geographic Information System (GIS) environment was generated and the DEM, the RGB and UV orthophotos were imported. Through the use of this tool, mainly using the DEM and the UV orthophotos as a further digital support, we generated polygons delimitating the different canvas and the restored parts on the RGB orthophoto. We also were able to map the principal alignments generated by topographic variations, color variations or a combination of both.

3. Results and discussion

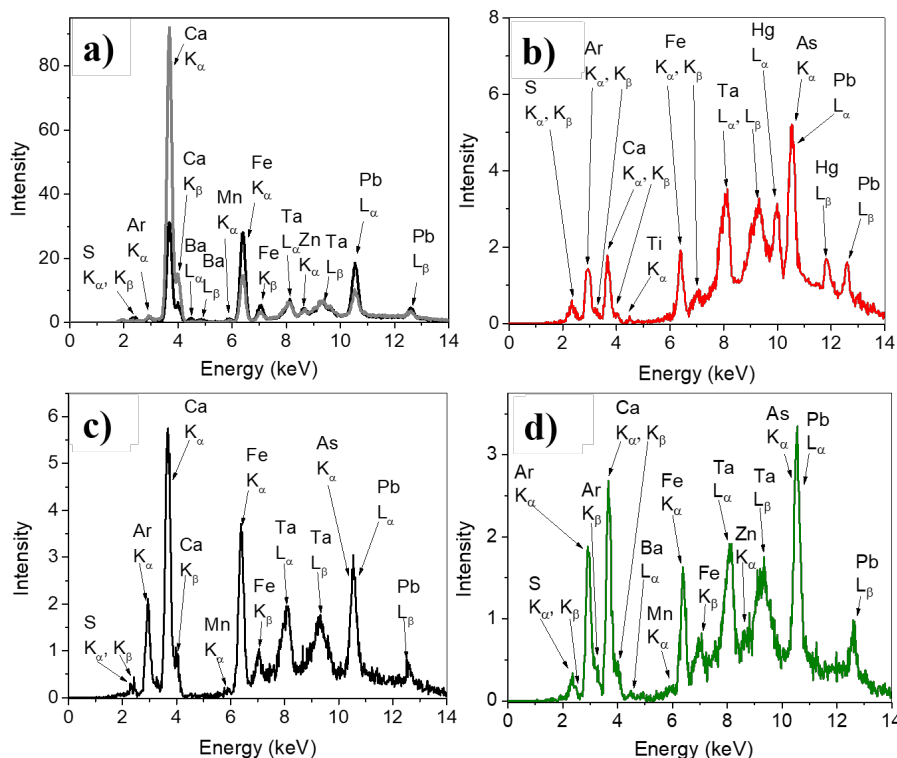
3.1 XRF analysis

XRF measurements on six different areas of the Lunette were carried out (Fig. 2, Table 1) in order to identify the elemental composition of superficial layer. Specifically, spectra were collected from points S1a and S1b, respectively associated to a light and a dark area of the canvas (the surface paint layer was, in these points, locally damaged), and from points S4, S5, S8 and S9, corresponding to red (S4), black (S5 and S8) and green-yellowish (S9) pigmented areas. The obtained elemental composition of the aforementioned areas is summarized in Table 2, whereas the obtained spectra, with the exception of spectrum of sample S8, that almost completely matched the spectrum of sample S5, are reported in Fig. 4.

Table 2 Elemental composition, as obtained by XRF data, of the analyzed points. The key elements for pigment identification are marked in bold. The minor or trace elements are presented between brackets

Point of analysis	XRF elemental composition
S1a	Ca, S, Pb, (Cl, Fe, K, Zn, Sr, Ba)
S1b	S, Ca, Pb, Cl, Fe, (As, K, Ba, Zn)
S4	S, Pb, Cl, As, Fe, Ca, K, Hg, (Sn, Cd)
S5	Ca, S, As, Fe, Pb, (Sr, Sb, Mn)
S8	S, Ca, Pb, As, Fe, (Sb, Mn, Sr)
S9	S, Ca, Pb, K, (Fe, As, Sb, Ba, Zn, Mn)

244



245

246

247

248

249

250

251

Fig. 4 XRF spectra, in the 0-14 keV range, collected on **a)** the light (point S1a, grey line) and dark (point S1b, black line) area on the right-side of the canvas, **b)** the red cloak of *St. Michael* (point S4, red line), **c)** the black wing of the angel on the left side of the painting (point S5, black line), and **d)** the green-yellowish sandalwood of *St. Michael* (point S9, green line)

252

A first inspection of Fig. 4a reveals, for both S1a and S1b points, the detection of S (K_{α} and K_{β} transition lines at ~ 2.31 keV and ~ 2.46 keV, respectively), Ca (K_{α} and K_{β} transition lines at ~ 3.68 keV and ~ 3.99 keV, respectively), Pb (L_{α} and L_{β} transition lines at ~ 10.55 keV and ~ 12.61 keV, respectively) and Fe (K_{α} and K_{β} at ~ 6.40 keV and ~ 7.05 keV, respectively). Their simultaneous presence suggests that the investigated surface can be attributed to a Ca-based and S-based preparatory layer, probably made of calcium carbonate (CaCO_3) and gypsum ($\text{CaSO}_4 \cdot 2\text{H}_2\text{O}$), mixed with a Fe-based compound, probably ochre (Fe_2O_3), lightened by a Pb-based compound, that could be lead white ($2\text{PbCO}_3 \cdot \text{Pb}(\text{OH})_2$), according to what reported in literature regarding Mattia Preti's execution technique (Hradil et al. 2020).

260

Moreover, being "oil on canvas" the painting technique used by Mattia Preti for the realization of the panel, the use of a Pb-based compound as dryer for the binder could be also reasonably hypothesized (Venuti et al. 2020). It is worth underlying that although sample S1b appeared, during the measurement acquisition, of an intense darkish-brownish coloration, the XRF spectrum collected on this area did not reveal any components attributable to pigments capable to offer dark shades/tonalities. The brownish color clearly visible to the naked eye could therefore be due to a natural oxidation of the investigated portion of the canvas, also considering that measurement was performed on a deteriorated area and taking into account the high amount of Pb detected.

266

267 In the case of the red area (Fig. 4b), the detected chemical elements suggested the use of Hg-/Fe-based
268 compounds, indicating that a mixture of cinnabar (HgS) and red ochre was probably employed. In addition, the
269 detection of Pb allows us to reasonably hypothesize the use of a Pb-based red (such as minium, Pb₃O₄) and/or
270 white (such as lead white) pigment, in order to obtain red/reddish tonalities, as those found in the bottom part of
271 the analysed cloak (see Fig. 2).

272 For what concerns the investigated black areas (S5 and S8), a comparable elemental composition can be
273 observed (see Table 2), suggesting the employment by Mattia Preti of a similar receipt for the blackish-brownish
274 tonalities. More in detail, the observation of high intensity peaks (Fig. 4c) at ~ 3.68 keV and ~ 3.99 keV,
275 respectively ascribed to the K_α and K_β transition lines of Ca, indicates the use of a typical Ca-based blackish
276 pigment of organic nature. It is reasonable to assume that the aforementioned pigmenting agent was also applied
277 as color background for other dark areas of the Lunette, including the entire upper-section of the painting, the *St.*
278 *Michael's* helmet and the wings of the angels. In this case, however, no further information can be obtained by
279 means of XRF spectroscopy, since the characteristic elements of such compound have a low Z number.
280 Nevertheless, the simultaneous detection of traces of Fe and Mn suggests that the organic black pigment was
281 probably mixed with natural umber (Fe₂O₃ + MnO₂ + nH₂O + Si + Al₂O₃), a common Fe/Mn-based dark-brownish
282 pigment.

283 As far as the XRF spectrum of the green-yellowish area is concerned (Fig. 4d), the detection of the
284 characteristic XRF transition lines of Fe and Pb indicates the application of a common Fe-based green pigment,
285 mixed, even in this case, with a Pb-based white compound (possibly lead white) in order to obtain different
286 shades/nuances. Going on, the observation of trace of Sb (see Table 2), in conjunction with Pb, suggests the
287 possible addition in the mixture of a Pb/Sb compound, probably Naples yellow, in order to obtain the observed
288 yellowish nuance. Worth of note, the experimental XRF spectrum of the green-yellowish area did not reveal any
289 contribution related to Cu, which leads us to exclude the use of a Cu-based green pigmenting agent in the painting,
290 although frequently applied at that time.

291 For all the investigated areas, the presence of Ba and Zn, when detected, indicates the possible application of
292 modern synthetic compounds, probably ascribed to previous restoration interventions (Feller 1986).

293 Finally, the presence of a significant amount of Ca in all the investigated areas deserves clarifications. In fact,
294 this occurrence supports the hypothesis regarding the presence of the typical globigerina limestone in the
295 preparatory layer of the painting (Hradil et al. 2020), whose observation appears crucial in order to ascribe the
296 investigated painting to the Maltese period of the artist. However, confirmation of this statement needs the
297 endorsement of complementary methodologies, being the distinction among different chemical compounds by
298 XRF analysis not possible.

299

300 3.2 Stereomicroscopic analysis

301

302 Stereomicroscopic investigations were conducted to closely examine the cross sections of the sampled micro-
303 fragments (see Fig. 5).

304



305

306

307 **Fig. 5** Images by stereomicroscope of the sampled micro-fragments

308

309 Sample S1b is completely impregnated, which makes the stratigraphy unclear with the exception of the most
310 superficial layer that appears of brownish color. Nevertheless, given the strong sample impregnation and

311 translucent appearance probably due to the use of different compounds (e.g. glues) in previous restoration
312 interventions, it is not clear whether the latter dark layer can be related to an alteration or to a superficial pictorial
313 film. Sample S2 is also impregnated, but shows three overlapping layers that, from the surface to the inside,
314 appear brownish, blackish and reddish in color, respectively. Sample S3 is the only one with clearer stratigraphy
315 and four visible layers. From the surface inwards, it is possible to distinguish a layer with blue pigments, followed
316 by a whitish layer, a blackish layer and a reddish one. Sample S4 shows three clearly visible layers, which from
317 the surface inwards range from a red layer, to a blackish layer and a reddish one in the lower portion. Samples S5-
318 S9 are all strongly impregnated samples with unclear stratigraphy, where only the superficial pictorial layer is
319 clearly visible. Specifically, S5 shows a pictorial blackish layer, S6 beige, S7 whitish-beige, S8 brownish-blackish,
320 and S9 green-yellowish. Regarding samples S10 and S11, they are also heavily impregnated, the stratigraphy is
321 not delineated and, furthermore, the painted surface layer is not visible.

322

323 3.3 SEM-EDX analysis

324

325 SEM-EDX investigations were conducted on 11 micro-fragments (see Table 1), investigating both the pictorial
326 layer and the underlying stratifications. A summary of the data is reported in Table 3, where the elemental
327 composition is shown for each sample analyzed.

328 EDX analyses, although semi-quantitative, can provide information on the artist's technique for the creation
329 of the canvas as well as identifying the presence of elements that could be associated to restorations carried out in
330 the past.

331 As for the composition of the layers under the painting film, for almost all the samples the presence of Ca, Pb
332 and Fe prevails (Table 3). Such composition clearly suggests that the preparatory layer could contain species
333 linked to these elements, such as calcium carbonate, lead white and red ochre (Fig. 6a-c). These data are in
334 agreement with the findings of the XRF survey.

335 It is worth to note that several studies report the use of such compounds during the Maltese period of Mattia
336 Preti (Lalli et al. 2014; Pelosi et al. 2018; D'Amico et al. 2019; Ridolfi 2019).

337 For some fragments, as in the case of sample S1b, it was possible to investigate the stratigraphy (Fig. 6d-i),
338 acquiring EDX maps in false colors. The maps better highlighted the artist's execution technique and the
339 application of the preparation layer on the canvas. The data acquired suggested that: a) the layer in contact with
340 the canvas, has a composition mainly based on Ca and Fe; b) the layer below the pictorial film shows the presence
341 of Pb and S. The use of pigments such as lead white, ochre and calcium carbonate could be hypothesized.
342 Furthermore, the presence, even if in low concentration, of Al, K, and Si (Table 3) is detected. These elements are
343 compatible with the presence of alunite ($KAl_3(SO_4)_2(OH)_6$) and silicates, commonly used by the artist for the
344 preparatory layers of his paintings on canvas (Hradil et al. 2020). Further morphological observations by SEM,
345 carried out in more detail on the layer in contact with the canvas, highlighted the presence of foraminifera and in
346 particular of the genus globigerina (Fig. 6l-n), with typical calcitic composition (Fig. 6o). The foraminifera
347 represents the fingerprint of the artist's Maltese production, deriving from the use of the local globigerina
348 limestone that Mattia Preti used to accentuate the red color for the preparation layer of his paintings. According
349 to the literature (Pelosi et al. 2018; D'Amico et al. 2019), Mattia Preti preferred the red color of the soil made by
350 microfossiliferous limestones, adding gypsum, alunite, opal, silicates, hematite and lead white.

351

Table 3. Summary of EDX elemental (weight %) analyses for all the samples

		O																		
		Ca	Si	S	Na	Mg	Al	Pb	Fe	Ba	Zn	Cl	P	K	Hg	Sb	Mn			
layer underneath the paint film	Sample S1b	29.79	52.55	0.97	2.03	0.44	0.30	10.29	1.40		0.83	0.40	1.00							
	Sample S2	33.65	45.19	8.16	3.69	1.79	1.18	1.92	31.99	2.16		0.27	1.99							
	Sample S4	33.24	34.01	5.64	4.06	2.60		5.21	11.64	1.00		1.10	1.50							
	Sample S6	33.32	48.58	5.19	2.77	2.60	0.52	1.39	2.44	1.80		0.37	0.42	0.60						
	Sample S8	35.30	29.86	12.92	1.43	1.20	0.82	2.29	6.44	7.50		0.47	0.47	1.30						
	Sample S10	30.68	34.64	3.00	4.16	3.77	0.53	1.47	5.59	5.55	5.65	1.96	0.73	0.58	1.69					
	Sample S11	30.20	30.32	3.18	4.64	3.68	0.96	1.62	6.57	3.97	8.37	2.00	1.64	0.68	2.17					
	Sample S1	27.20	24.37	2.96	4.36	1.10	0.31	1.45	23.28	5.67	4.21	2.92	1.04	0.76	0.37					
	Sample S2	31.90	18.03	2.99	6.21	0.63	3.08	1.44	22.07	3.09	3.92	3.92	1.44	0.71	0.57					
	Sample S3	29.99	34.15	0.93		0.48	0.61	0.85	22.99	10.00										
	Sample S4	19.88	8.54	1.23	15.72	1.31	0.22	0.95	20.90	0.79		0.43	0.53	2.14	27.36					
Sample S5	36.15	34.73	3.04	4.05		0.72	1.01	18.20					2.11							
Sample S6	20.55	22.30	5.84	3.85	0.86	0.34	3.04	33.91	3.54	2.66	1.14	0.63	0.28	1.06						
Sample S7	20.70	24.01	5.73	5.72	0.58	1.00	3.24	33.88	3.81			0.50		0.83						
Sample S8	18.57	11.25	3.49	1.54	1.01	0.34	1.25	57.58	2.65	0.75			0.47	1.10						
Sample S9	24.64	13.55	3.82	5.54	1.52	0.99	0.61	38.93	2.66	2.91		1.12		3.71						
Sample S10	28.21	29.83	6.30	3.46	2.12	0.60	2.43	10.13	7.32	3.15	1.48	0.91	0.69	1.98				1.39		
Sample S11	29.51	27.08	7.16	2.45	2.25	0.89	3.45	11.25	8.04	1.94	1.16	0.69	0.89	1.75				1.49		

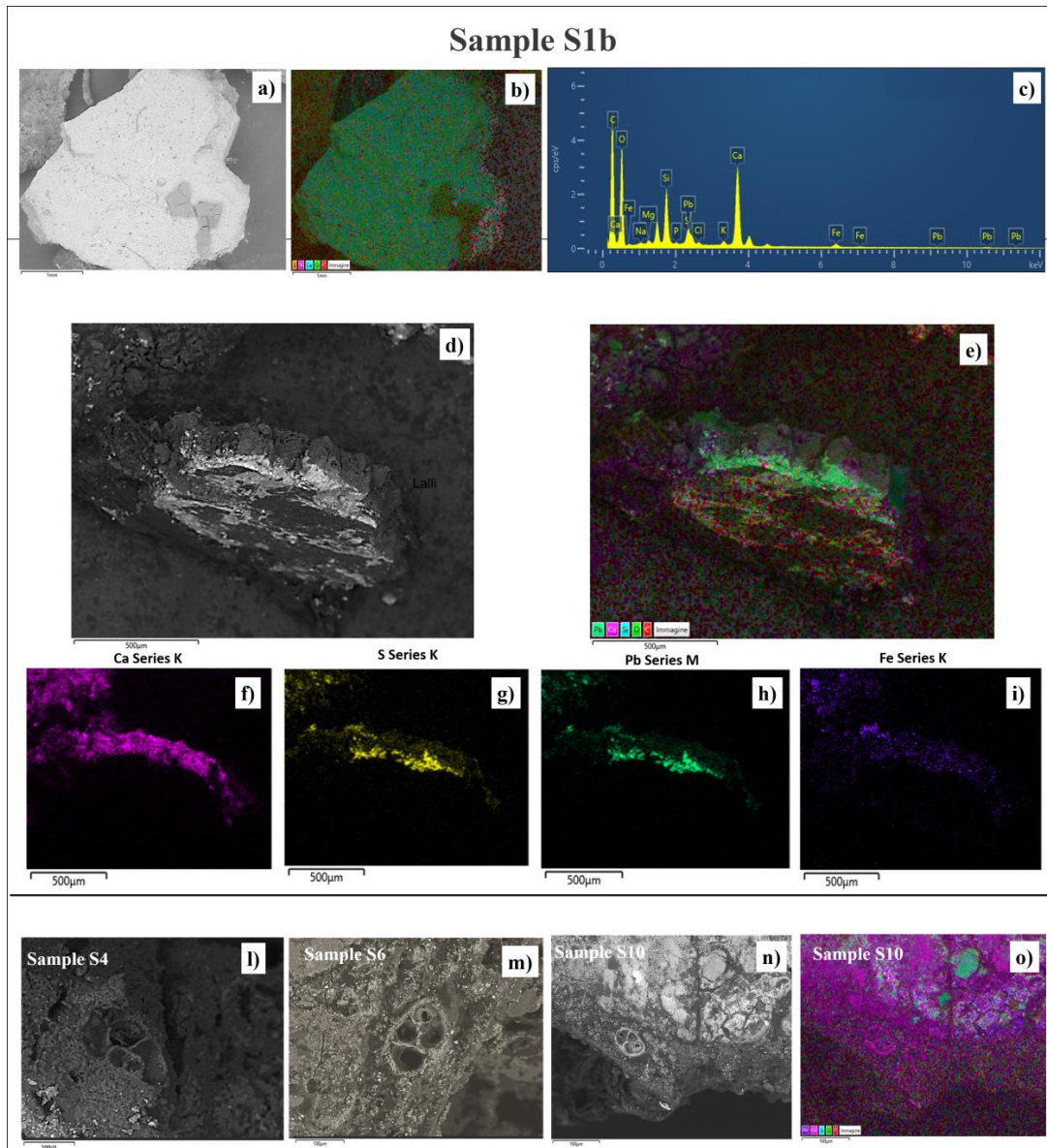
355
356

Fig. 6 SEM images showing the layers below the pictorial film of some samples. **a)** Back-Scattered Electrons (BSE) image of sample S1b; **b)** SEM-EDX false-color map obtained from the analysis of the surface of sample S1b; **c)** EDX spectrum obtained from the analyzed surface of sample S1b, **d)** BSE image of sample S1b placed vertically to the painting surface; **e)** false-color map obtained from the analysis of the surface of sample S1b placed vertically to the sampled surface; **f)** SEM-EDX false color map of Ca; **g)** SEM-EDX false color map of S; **h)** SEM-EDX false color map of Pb; **i)** SEM-EDX false color map of Fe; **l)** BSE image of globigerina observed in sample S4; **m)** BSE image of globigerina observed in sample S6; **n)** BSE image of globigerina observed in sample S10; **o)** SEM-EDX false color map of sample S10 where globigerina was observed

365

366

As regards sample S2, the EDX investigations on the pictorial layer showed a high Pb content, thus allowing us to hypothesize the use of a lead white also as a pigmenting agent and not only for the preparatory layer of the canvas.

367

368

369

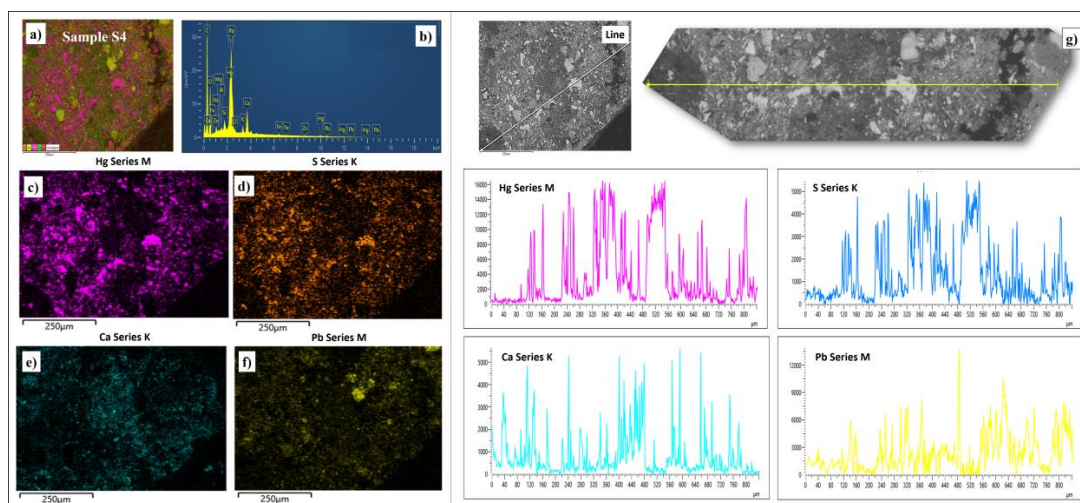
For samples S3, S5 and S8 it was not possible to hypothesize specific pigments, in agreement with what was already observed, in the case of sample S5 and S8, by XRF analysis. In fact, in line with the first observations performed by stereomicroscope, the pictorial surfaces showed a blue color for the sample S3, while for S5 and S8

370

371

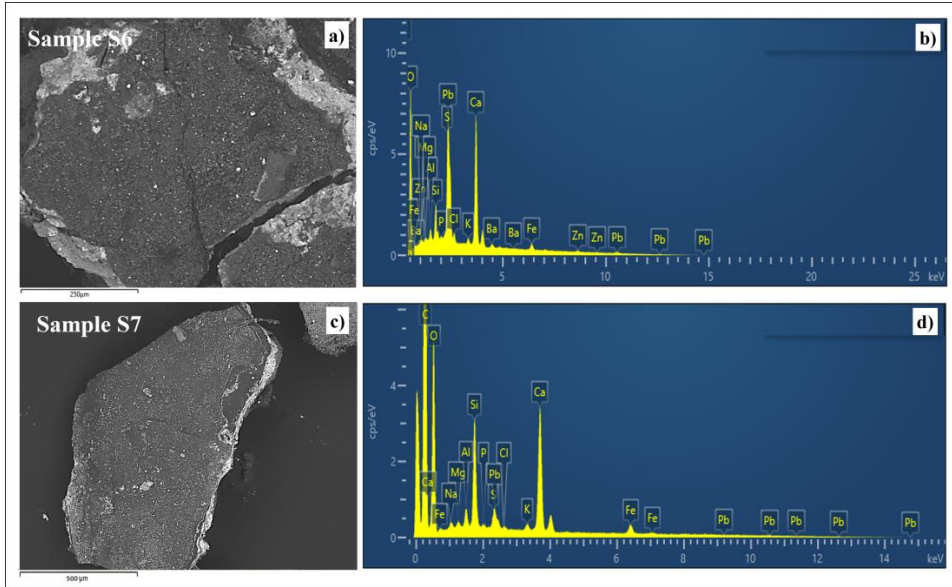
372 a brown-blackish and black color respectively. It is known that Mattia Preti used pigments such as carbon black,
 373 vine black, black bone (Chiavari et al. 2007; Lalli et al. 2014; Pelosi et al. 2018; Hradil et al. 2020) for the black
 374 color, while blue glaze, indigo or lapis (Chiavari et al. 2007; Pelosi et al. 2018; Ridolfi 2019) for blue pigments.
 375 Nevertheless, the elements indicative of the presence of these pigments were not highlighted.

376 As for the S4 sample, that appeared red by the stereomicroscope observations, the EDX analyses showed high
 377 concentrations of S, Hg, Pb and Ca (Table 3, Fig. 7), which suggest the use of cinnabar, as also hypothesized by
 378 XRF analysis, and of minium, both pigments used together in the palette of Mattia Preti to paint red surfaces
 379 (Chiavari et al. 2007; Pelosi et al. 2018). On sample S4, EDX maps were acquired in false colors (Fig. 7a-f),
 380 confirming that the entire surface is composed of the aforementioned elements. Further investigations, by
 381 performing an EDX analysis following a linear trajectory along the sample surface (Fig. 7g), revealed similar
 382 profiles of Hg (series M) and S (series K), confirming the presence of HgS. On the contrary, those of Ca (K series)
 383 and Pb (M series) appear different, suggesting that lead is present on the surface as a pigment different from lead
 384 white (probably minium).
 385



386
 387
 388 **Fig. 7** SEM- EDX images showing the analysis of sample S4. **a)** SEM-EDX false-color map obtained from the
 389 analysis of the surface of sample S4, **b)** EDX spectrum obtained from the analyzed surface of sample S4, **c)** SEM-
 390 EDX false-color map of Hg, **d)** SEM-EDX false-color map of S, **e)** SEM-EDX false-color map of Ca, **f)** SEM-
 391 EDX false-color map of Pb, **g)** EDX analysis following a linear trajectory performed on the surface of sample S4,
 392 with associated profilometry spectra of Hg, S, Ca and Pb
 393

394 Samples S6 and S7, taken from two different areas of the incarnates, respectively those of the angel on the left
 395 of the canvas (S6) and from St. Michael (S7), show an almost similar chemical composition of the pictorial layer
 396 with high concentrations of Pb and Ca and lower quantities of Si, Al and Fe. The chemical composition detected
 397 by EDX suggests, on the basis of the elements characteristic of the corresponding pigments, the use of a mixture
 398 composed of lead white added to red lead and green earth, pigments used by Mattia Preti to reproduce a skin color
 399 (Lalli et al. 2014). The only difference in the chemical composition of S6 and S7 (Fig. 8) is the presence of low
 400 concentrations of Ba and Zn (Table 3), the latter found only in S6 (and also in other samples as reported in Table
 401 3).
 402



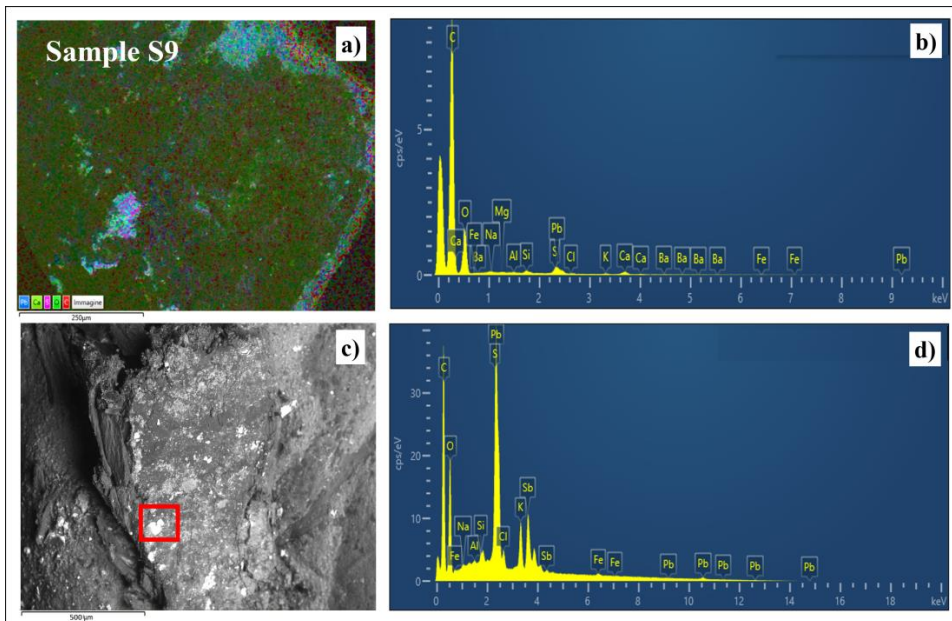
403
404
405
406
407
408

Fig. 8 SEM- EDX images showing the analysis of sample S6 and S7. **a)** BSE image of sample S6, **b)** EDX spectrum obtained from the analysed surface of sample S6, **c)** BSE image of sample S7, **d)** EDX spectrum obtained from the analysed surface of sample S7

409
410
411
412
413
414
415
416
417
418
419
420

The presence of Ba and Zn on the pictorial surface in some specific points confirms that the canvas has undergone restoration work in the past. In fact, these two elements can be due to the use of zinc white (ZnO) and barium white (BaSO₄) or to the use of lithopone, i.e. a white composed of barium sulfate and zinc sulphide (BaSO₄ + ZnS), pigments produced since the end of the 19th century.

As for the EDX analysis performed on the S9 sample, it allowed us to support the use of Naples yellow pigment, also known as “Giallo d'Antimonio”, among the most used yellow pigments in Mattia Preti's palette (Ridolfi 2019; Hradil et al. 2020), as already suggested by the XRF composition collected on the same point. In this regard, Pb and Sb were, in particular, detected (Table 3, Fig. 9a,b) on single particles, such as that shown in Fig. 9c, whose EDX spectrum is reported in Fig. 9d. Interestingly, low amount of Fe can be recognized, in agreement with XRF results, indicating the possible addition of a Fe-based pigment in order to obtain different green-yellowish shades/nuances.



421

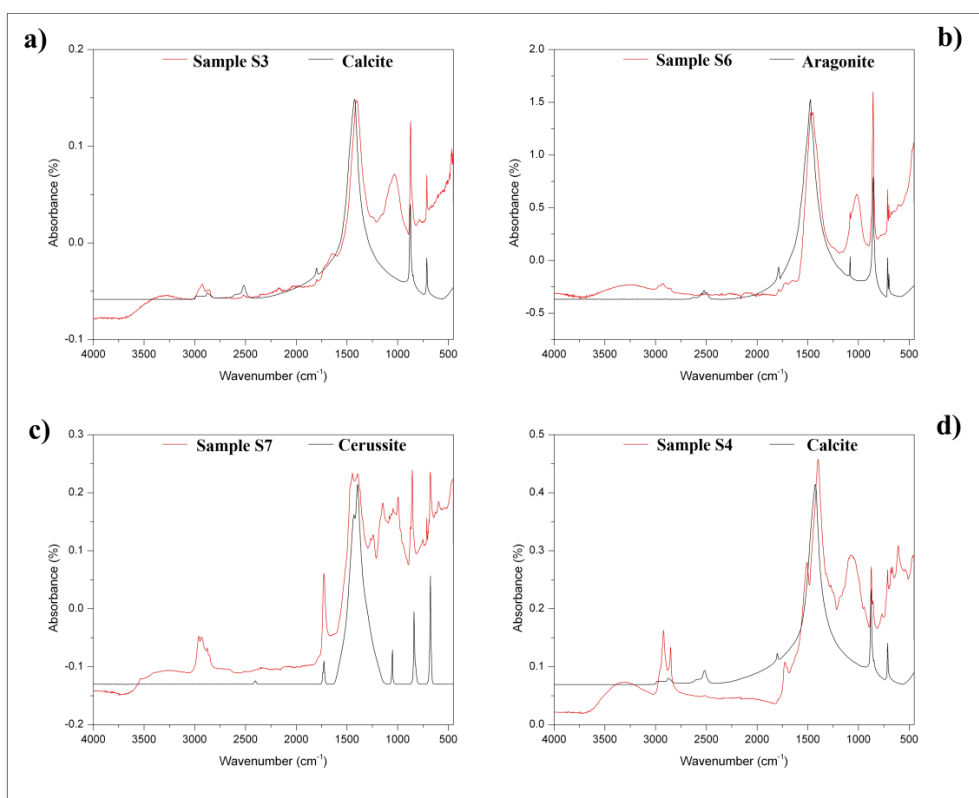
422
423
424
425
426
427
428
429
430
431
432
433
434
435
436
437
438
439

Fig. 9 SEM- EDX images showing the analysis of sample S9. **a)** SEM-EDX false color map obtained from the analysis of the surface of sample, **b)** EDX spectrum obtained from the analyzed surface, **c)** BSE image of an area of sample S9 (the red rectangle indicates the analyzed area), **d)** EDX spectrum obtained from the analyzed area

Lastly, the brownish colored samples S10 and S11, as evidenced by the observations by stereomicroscopy, show a similar chemical composition, which is typical of the use of Sienna, a color composed of iron oxides, clay silicates and small amount of manganese dioxide, probably mixed with lead white (the presence of all these species is suggested by the elemental composition highlighted). In fact, high concentrations of Ca and Pb (Table 3) were detected, followed by Al, Si and Fe, and low concentrations of Mn.

3.4 FT-IR analysis

Infrared spectroscopy was essentially addressed at characterizing the main inorganic materials (i.e. mineralogical phases) within the samples. All the analyses are referred to the whole sample, since it was not possible to isolate the surface from the bulk and the various layers, nor much less the sample was ground, given its very small size, fragility and the risk of completely losing material. Some representative spectra are reported in Fig. 10.



440
441
442
443
444
445
446
447
448
449
450
451
452
453
454

Fig. 10 Representative FT-IR absorbance spectra of the **a)** S3, **b)** S6, **c)** S7 and **d)** S4 samples

In all analysed samples, the stretching vibrations of calcite, peaked at ~ 1409 , ~ 875 and ~ 711 cm^{-1} were identified (Derrick et al. 2000; Vahur et al. 2016), supporting the thesis that the artist used the globigerina limestone, the typical oligo-Miocene limestone of Malta, in the preparatory layers. This thesis can be further confirmed as in some samples (i.e. samples S6 and S9) aragonite (i.e. a polymorph of calcium carbonate) has been identified (peaks respectively at ~ 1788 , ~ 1473 , ~ 1082 , ~ 906 , ~ 854 , ~ 712 and ~ 699 cm^{-1}) (Linga Raju et al. 2002), as a consequence of the dissolution of calcium carbonate skeletal fragments and typical of the skeletal structures of organisms such as foraminifera (globigerina). Overall, calcite and aragonite have to be considered as binder phases, because the majority of the matrix is composed by calcium carbonates as also suggested by the SEM-EDX analysis. Of course, both phases may have also been used as white pigments; based on the fact that aragonite was often used in association with cinnabar in order to “dilute” the red color, or with other pigments to tone down the color and to dose the shade, or to prepare a white base (Angelini et al. 2019).

455 The absorbance band, which is strong in all the samples, peaked at $\sim 1020 \text{ cm}^{-1}$ is ascribable to the stretching
 456 of Si-O bond, indicating silicate compounds, probably deriving from sandy raw materials used as inert in the
 457 preparatory layers or as pigmenting agent.

458 The presence of cerussite (i.e. lead carbonate, PbCO_3) was also detected in samples S7, with typical peaks at,
 459 ~ 1432 , ~ 1394 , ~ 1051 , ~ 838 , $\sim 677 \text{ cm}^{-1}$. It is indicative of the probable use of lead white, one of the most
 460 widely used white pigments in the past, mainly because of its high opacity and hiding power (Learner 2007; de
 461 Viguerie et al. 2018; Gonzalez et al. 2019).

462 Finally, taking into account the hypothesis deduced from the XRF and SEM-EDX investigations, related to
 463 S6, S7 and S9, no bands attributable to green earth have been identified.

464 In addition to inorganic compounds, samples showed the stretching bands of the carboxylic (-COOH) group
 465 peaked at $\sim 1700 \text{ cm}^{-1}$, particularly evident in sample S7, and those of the stretching of C-H group at ~ 2852 and
 466 $\sim 2922 \text{ cm}^{-1}$, suggesting the presence of an organic matter which is probably highly related with the binder. In the
 467 case of sample S4 the band at $\sim 1700 \text{ cm}^{-1}$ is present together with a band at about 1530 cm^{-1} that could be due to
 468 the amide group (Fermo et al. 2020) (the third typical amide band is at about 1440 cm^{-1} , but it is below the
 469 carbonate signal); these signals are therefore due to amino acids present confirming the presence of a protein-type
 470 ligand.

471

472 3.5 GC-MS analysis

473

474 GC-MS analyses were carried out only on samples S3 and S7. Both fatty acids and amino acids were detected in
 475 both samples. Thanks to the comparison with references values reported in the literature (Casoli et al. 1996;
 476 Colombini et al. 1998, 1999), the presence of linseed oil and an animal glue were disclosed. The animal glue was
 477 probably present in the preparatory layer underneath the painting film, while the siccative oil was employed as
 478 binder. This is in accordance with what already found for other paintings by Mattia Preti (Chiavari et al. 2007).
 479 This preliminary study deserves further investigation by expanding the number of samples.

480

481 3.6 3D photogrammetric survey

482

483 Three different canvases as well as the areas that experienced previous restorations were identified and mapped.
 484 Each of these areas have characteristic features, as “geographic” distribution, topographic position, texture, RGB
 485 range of colors and response to the UV light (Fig. 11a). Canvas 1 represents the canvas where the original paint
 486 is located. It has a central position in the painting and, clearly, presents restored parts. The restored part represents
 487 the restoration stucco, used to complete the missing parts of the Canvas 1 (Fig. 11b, c). It is interesting to see how
 488 this restored parts (which represent parts were the original paint were damaged) have got lineal patrons. Canvas
 489 2 is a canvas under the Canvas 1 and used in a previous and old restoration phase. Presumably, the actual total
 490 size of this canvas is bigger than the Canvas 1, but it is covered by it, so the exposed area is relatively small.
 491 Canvas 3 lays under Canvas 1 and Canvas 2, in contact with the latter. As Canvas 2, the majority of its area is
 492 covered, and it is well exposed in the borders of the painting. Table 4 shows the size of the total and the visible
 493 areas of the different canvases, extracted from the GIS analysis.

494

495 **Table 4** Results extracted from GIS analysis

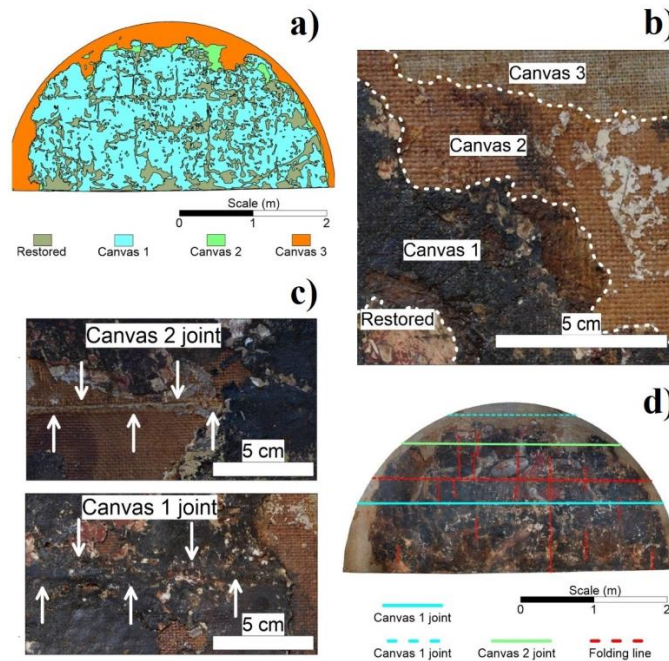
496

	Total Area (sq m)	Total Area (%)	Visible Area (sq m)	Visible Area (%)
Canvas 3	8.39	100	1.38	16.47
Canvas 2	7.01	83.53	2.35	28.01
Canvas 1	4.66	55.52	2.85	33.99
Restored	1.81	21.53	1.81	21.53
Restored area in relation with Canvas 1 (%)	38.78			

497

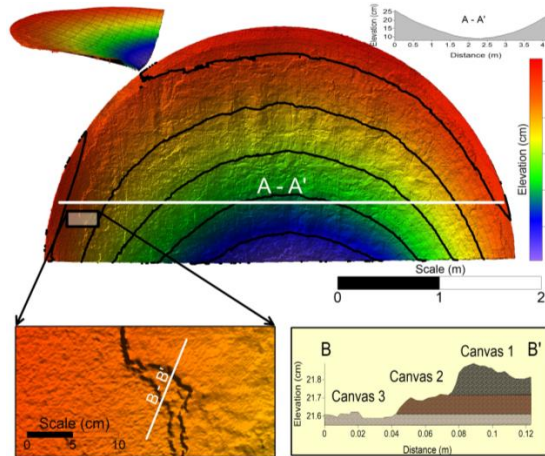
498 During the analysis of the reconstructed 3D digital model, it was possible to recognize on the painting different
 499 kinds of alignments (Fig. 11d). Those parts are different in color, texture and topographical features. In light blue
 500 we marked a horizontal line approximately in the middle of the painting. This line is pointing an alignment
 501 affecting just the Canvas 1. It is interpreted as a merging feature within the Canvas 1. The upper light blue dashed

502 line (inferred position) is located parallel to the first one and separated of about 1.20 m. In this region, Canvas 1
 503 is not visible, thus we located the potential position of the merged canvases taking into account the position of the
 504 main join as well as the size of the typical canvas at the time of Mattia Preti available in Malta and southern Italy.
 505 The green line is interpreted as an internal union of the Canvas 2. This union is very evident and directly visible,
 506 and it affects neither Canvas 1 nor Canvas 3. The lines in red are placed where the original painting was damaged,
 507 and we interpreted them as a weakness line. They are distributed both in the horizontal and vertical directions.
 508 We interpret those features as sign of folding of the painting. In fact, historical fonts report that the painting has
 509 been folded a couple of times, the latter during the Second World War, when the painting was stored away and
 510 kept in a secure place. The folding was done probably first in the horizontal direction, and then the painting was
 511 rolled, causing the damage in the vertical direction.
 512



513
 514 **Fig. 11** Results of the interpretation obtained using the digital 3D model. **a)** Mapping of the three different
 515 canvases and restored areas. Panels **b)-d)** show details of the painting highlighting the different types of canvas
 516 as well as the joints between them
 517
 518

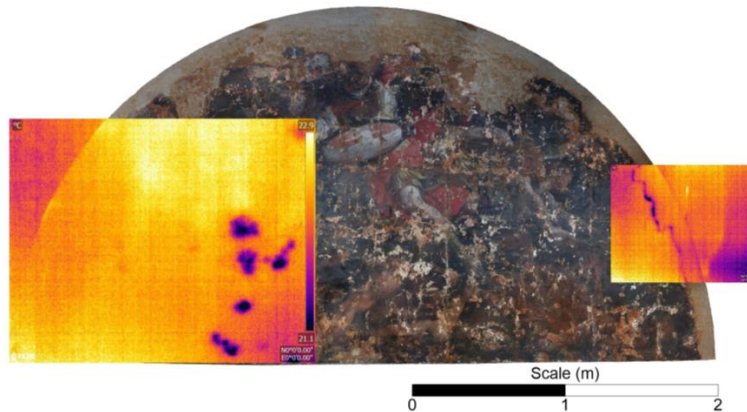
519 The topographical/morphological analysis (Fig. 12) revealed the external “U” shape of the Lunette, being
 520 flatted on the boarder. This “U” shape is less evident near to the top of the painting. The difference between the
 521 highest part on the edges and lowest part on the low center of the painting turned out to be 28 cm. The construction
 522 of the frame following this shape was necessary in order to accommodate the painting in its present location. This
 523 analysis, together with the 3D model (Fig. 3), will allow to print the frame with exactly the same features and
 524 measurements in case of any damage to the structure. The high resolution DEM also allowed us to do observations
 525 at more detailed scale. At millimetric scale, it was possible to discriminate among the three different canvas
 526 and to determinate the thickness of the Canvas 1 (between 1 and 1.5 mm), with a relatively thick paint layer, and of
 527 the Canvas 2 (1 mm), without any paint.
 528



529
530

531 **Fig. 12** Reconstructed DEM of the painting. The top panel shows the high precision model of the entire artefact
532 as well as its curvature. Bottom panel shows a detail of the model where the 3 different canvases can be identified;
533 the sketch on the right reports a schematic reconstruction
534

535 Finally, during the restoration a thermal camera was used to monitor the application of consolidation material
536 (Fig. 13) used to strengthen the painting. In particular, different injection points of such consolidating media were
537 revealed, identified as the dark spots/areas in thermal images. In the future, such kind of approach can be used in
538 real-time to monitor each phase of the restoration works with the aim of optimizing the timing of the different
539 phases.
540



541
542

543 **Fig. 13** Thermal image of the painting during the restoration
544

545 4. Concluding remarks

546

547 In the present work, a combined approach involving non-invasive optical and physical/chemical analysis, ranging
548 from elemental to molecular scale, and 3D digital survey, was successfully applied on the large *St. Michael*
549 *defeating Evil* painting by Mattia Preti, located inside the Church of the Immaculate Conception of Sarria
550 (Floriana) in Malta. In particular, the combined use of XRF, SEM-EDX, FT-IR and GC-MS techniques allowed
551 us to identify, starting from the evaluation of elemental/molecular compositions, the pigmenting agents,
552 preparatory and organic binding materials used by the artist, so providing a better understanding of the execution
553 technique, the pigment's palette and the occurrence of non-documented restoration treatments. In this context,
554 random interventions were testified by the detection of elements generally associated to modern/synthetic media.
555 In addition, measurements allowed us to confirm, among other aspects, the use by Mattia Preti of the typical
556 Maltese globigerina limestone as main component for the painting ground, furnishing an experimental evidence
557 of the Maltese origin of the investigated painting. This also contributes to temporally locate the investigated
558 Lunette to the Maltese period of the artist, which was, up to now, still unverified. On the other side, the obtained
559 3D digital models of the painting allowed us to quantify the extension of damaged parts, to map the domains of

560 the different canvases employed, to derive its state of conservation and to highlight possible additions made during
561 previous non-documented restorations. These aspects, along with the characterization of the materials through
562 complementary methodologies, contribute to support/plan future restoration and intervention strategies to be
563 applied.

564 **Declarations**

565

566 **Acknowledgements**

567

568 The authors are grateful to Dott. Mattia Casanova and to Shimadzu Italia srl for the support in GC-MS analysis.
569 The authors kindly acknowledge Dr. Massimo Tagliaferro and Nanovision S.r.l. (Italy) for the scientific support
570 and for having provided us with the Hitachi TM-4000 instrument.

571

572 **Ethics approval and consent to participate**

573

574 Not applicable.

575

576 **Consent for publication**

577

578 Not applicable.

579

580 **Availability of data and materials**

581

582 All data generated or analyzed during this study are included in this published article.

583

584 **Competing interests**

585

586 The authors declare that they have no competing interests.

587

588 **Authors' contributions**

589

590 S. D'Amico, S. Guido, G. Mantella, V. Venuti performed sampling. S. D'Amico, E. Colica and L. Galone carried
591 out the 3D photogrammetric survey. V. Comite, P. Fermo carried out SEM-EDX and GC-MS investigation. G.
592 Paladini, V. Crupi, D. Majolino, V. Venuti carried out XRF investigation. M. Ricca, M. F. La Russa, L. Randazzo
593 carried out stereomicroscopic analysis and FT-IR investigation. S. Guido, G. Mantella provided all information
594 regarding the historic-artistic context. S. D'Amico, V. Comite, G. Paladini, M. Ricca, V. Venuti wrote the
595 manuscript. All authors read and approved the final manuscript.

596

597 **References**

598

- 599 Aicardi I, Chiabrando F, Maria Lingua A, Noardo F (2018) Recent trends in cultural heritage 3D survey: The
600 photogrammetric computer vision approach. *J Cult Herit* 32:257–266.
601 <https://doi.org/10.1016/j.culher.2017.11.006>
- 602 Angelini I, Asscher Y, Secco M, Parisatto M, Artioli G (2019) The pigments of the frigidarium in the Sarno Baths,
603 Pompeii: Identification, stratigraphy and weathering. *J Cult Herit* 40:309–316.
604 <https://doi.org/10.1016/j.culher.2019.04.021>
- 605 Arias P, Armesto J, Di-Capua D, González-Drigo R, Lorenzo H, Pérez-Gracia V (2007) Digital photogrammetry,
606 GPR and computational analysis of structural damages in a mediaeval bridge. *Eng Fail Anal* 14:1444–1457.
607 <https://doi.org/10.1016/j.engfailanal.2007.02.001>
- 608 Armesto J, Arias P, Roca J, Lorenzo H (2008) Monitoring and Assessing Structural Damage in Historic Buildings.
609 *Photogramm Rec* 23:36–50. <https://doi.org/10.1111/j.1477-9730.2008.00466.x>
- 610 Balletti C, Beltrame C, Costa E, Guerra F, Vernier P (2016) 3D reconstruction of marble shipwreck cargoes based
611 on underwater multi-image photogrammetry. *Digit Appl Archaeol Cult Herit* 3:1–8.
612 <https://doi.org/10.1016/j.daach.2015.11.003>
- 613 Barbera G, Barone G, Crupi V, Longo F, Majolino D, Mazzoleni P, Sabatino G, Tanasi D, Venuti V (2012) Study
614 of Late Roman and Byzantine glass by the combined use of analytical techniques. *J Non Cryst Solids*
615 358:1554–1561. <https://doi.org/10.1016/j.jnoncrsol.2012.04.013>
- 616 Bersani D, Berzioli M, Caglio S, Casoli A, Lottici PP, Medeghini L, Poldi G, Zannini P (2014) An integrated
617 multi-analytical approach to the study of the dome wall paintings by Correggio in Parma cathedral.
618 *Microchem J* 114:80–88. <https://doi.org/10.1016/j.microc.2013.11.014>
- 619

620 Bersani D, Lottici PP, Casoli A, Cauzzi D (2008) Pigments and binders in “Madonna col Bambino e S.
621 Giovannino” by Botticelli investigated by micro-Raman and GC/MS. *J Cult Herit* 9:97–102.
622 <https://doi.org/10.1016/j.culher.2007.05.005>

623 Casoli A, Musini PC, Palla G (1996) Gas chromatographic-mass spectrometric approach to the problem of
624 characterizing binding media in paintings. *J Chromatogr A* 731:237–246. [https://doi.org/10.1016/0021-](https://doi.org/10.1016/0021-9673(95)01194-3)
625 [9673\(95\)01194-3](https://doi.org/10.1016/0021-9673(95)01194-3)

626 Castro K, Ábalos B, Martínez-Arkarazo I, Etxebarria N, Madariaga JM (2008) Scientific examination of classic
627 Spanish stamps with colour error, a non-invasive micro-Raman and micro-XRF approach: The King
628 Alfonso XIII (1889-1901 “Pelón”) 15 cents definitive issue. *J Cult Herit* 9:189–195.
629 <https://doi.org/10.1016/j.culher.2008.02.001>

630 Chiavari G, Prati S, Lanterna G, Lalli C, Cagnini A (2007) Diagnostic study of the materials and painting
631 techniques in “The Dinner of Emmaus” by Gregorio (and Mattia?) Preti. *Microchim Acta* 159:357–362.
632 <https://doi.org/10.1007/s00604-007-0759-2>

633 Colica E, Micallef A, D’Amico S, Cassar LF, Galdies C (2018) Investigating the Use of UAV Systems for
634 Photogrammetric Applications: A Case Study of Ramla Bay (Gozo, Malta). *J Malta Chamb Sci* 5:125–131.
635 <https://doi.org/10.7423/XJENZA.2017.2.04>

636 Colombini MP, Fuoco R, Giacomelli A, Muscatello B (1998) Characterization of Proteinaceous Binders in Wall
637 Painting Samples by Microwave-Assisted Acid Hydrolysis and GC-MS Determination of Amino Acids.
638 *Stud Conserv* 43:33. <https://doi.org/10.2307/1506634>

639 Colombini MP, Modugno F, Giacomelli A (1999) Two procedures for suppressing interference from inorganic
640 pigments in the analysis by gas chromatography–mass spectrometry of proteinaceous binders in paintings.
641 *J Chromatogr A* 846:101–111. [https://doi.org/10.1016/S0021-9673\(99\)00192-2](https://doi.org/10.1016/S0021-9673(99)00192-2)

642 Comite V, Ricca M (2016) Diagnostic investigation for the study of the fresco “Madonna con il bambino”, from
643 Cosenza, southern Italy: a case study. *Rend Online della Soc Geol Ital* 38:21–24.
644 <https://doi.org/10.3301/ROL.2016.07>

645 Crupi V, Fazio B, Fiocco G, Galli G, La Russa MF, Licchelli M, Majolino D, Malagodi M, Ricca M, Ruffolo SA,
646 Venuti V (2018) Multi-analytical study of Roman frescoes from Villa dei Quintili (Rome, Italy). *J Archaeol*
647 *Sci Reports* 21:422–432. <https://doi.org/10.1016/j.jasrep.2018.08.028>

648 D’Amico S, Saccone M, Persico R, Venuti V, Spagnolo G V, Crupi V, Majolino D (2017) 3D survey and GPR
649 for cultural heritage. The case study of SS. Pietro and Paolo Church in Casalvecchio Siculo. *Kermes* 107:11–
650 15

651 D’Amico S, Venuti V, Colica E, Paladini G, Galone L, Crupi V, Majolino D, Guido S, Mantella G (2020) Digital
652 reconstruction and scientific analysis prior the restoration of two paintings by Mattia Preti in the Church of
653 the Immaculate Conception of Sarria (Floriana, Malta). In: 2020 IMEKO TC-4 International Conference on
654 Metrology for Archaeology and Cultural Heritage. pp 532–537

655 D’Amico S, Venuti V, Colica E, Crupi V, Majolino D, Paladini G, Guido S, Mantella G, Zumbo R (2019)
656 Scientific investigation of the Conversion of St Paul painting (Mdina, Malta). In: 2019 IMEKO TC-4
657 International Conference on Metrology for Archaeology and Cultural Heritage. pp 330–334

658 de Viguier L, Glanville H, Ducouret G, Jacquemot P, Dang PA, Walter P (2018) Re-interpretation of the Old
659 Masters’ practices through optical and rheological investigation: The presence of calcite. *Comptes Rendus*
660 *Phys* 19:543–552. <https://doi.org/10.1016/j.crhy.2018.11.003>

661 Derrick MR, Stulik D, Landry JM (2000) *Infrared spectroscopy in conservation science*. Getty Publications

662 Edwards HGM, Jorge Villar SE, Eremin KA (2004) Raman spectroscopic analysis of pigments from dynastic
663 Egyptian funerary artefacts. *J Raman Spectrosc* 35:786–795. <https://doi.org/10.1002/jrs.1193>

664 Feller RL (1986) Barium sulfate - natural and synthetic. In: *Artists’ pigments: a handbook of their history and*
665 *characteristics*. pp 47–64

666 Fermo P, Mearini A, Bonomi R, Arrighetti E, Comite V (2020) An integrated analytical approach for the
667 characterization of repainted wooden statues dated to the fifteenth century. *Microchem J* 157:105072.
668 <https://doi.org/10.1016/j.microc.2020.105072>

669 Fiorillo F, Jiménez Fernández-Palacios B, Remondino F, Barba S (2015) 3d Surveying and modelling of the
670 Archaeological Area of Paestum, Italy. *Virtual Archaeol Rev* 4:55. <https://doi.org/10.4995/var.2013.4306>

671 Gonzalez V, Wallez G, Calligaro T, Gourier D, Menu M (2019) Synthesizing lead white pigments by lead
672 corrosion: New insights into the ancient manufacturing processes. *Corros Sci* 146:10–17.
673 <https://doi.org/10.1016/j.corsci.2018.10.033>

674 Hradil D, Hradilová J, Lanterna G, Galeotti M, Holcová K, Jaques V, Bezdička P (2020) Clay and alunite-rich
675 materials in painting grounds of prominent Italian masters – Caravaggio and Mattia Preti. *Appl Clay Sci*
676 185:105412. <https://doi.org/10.1016/j.clay.2019.105412>

677 La Russa MF, Ruffolo SA, Belfiore CM, Comite V, Casoli A, Berzioli M, Nava G (2014) A scientific approach
678 to the characterisation of the painting technique of an author: the case of Raffaele Rinaldi. *Appl Phys A*
679 114:733–740. <https://doi.org/10.1007/s00339-013-7866-1>

680 Lalli CG, von Breska-Ficović N, Innocenti F, Kolić Pustičić M (2014) Le due serie dei quattro “Evangelisti” di
681 Mattia Preti a Dubrovnik: un progetto multidisciplinare e di collaborazione tra il Laboratorio Scientifico
682 dell’Opificio e l’Istituto Croato di RestauroSource: OPD Restauro. Cent Di Della Edifimi SRL 26:231–248
683 Learner T (2007) Modern paints: uncovering the choices. In: Modern paints uncovered: proceedings from the
684 modern paints uncovered symposium
685 Linga Raju C, Narasimhulu K., Gopal N., Rao J., Reddy BC. (2002) Electron paramagnetic resonance, optical
686 and infrared spectral studies on the marine mussel *Arca burnesi* shells. *J Mol Struct* 608:201–211.
687 [https://doi.org/10.1016/S0022-2860\(01\)00952-8](https://doi.org/10.1016/S0022-2860(01)00952-8)
688 Pelosi C, Agresti G, Baraldi P (2018) The ‘slash of light’ in the late religious paintings of Mattia Preti technique
689 and materials. *Eur J Sci Theol* 14:151–160
690 Remondino F (2011) Heritage recording and 3D modeling with photogrammetry and 3D scanning. *Remote Sens*
691 3:1104–1138. <https://doi.org/10.3390/rs3061104>
692 Remondino F, Girardi S, Rizzi A, Gonzo L (2009) 3D modeling of complex and detailed cultural heritage using
693 multi-resolution data. *J Comput Cult Herit* 2:1–20. <https://doi.org/10.1145/1551676.1551678>
694 Ricca M, Paladini G, Rovella N, Ruffolo SA, Randazzo L, Crupi V, Fazio B, Majolino D, Venuti V, Galli G, La
695 Russa MF (2019) Archaeometric Characterisation of Decorated Pottery from the Archaeological Site of
696 Villa dei Quintili (Rome, Italy): Preliminary Study. *Geosciences* 9:172.
697 <https://doi.org/10.3390/geosciences9040172>
698 Ridolfi S (2019) Relazione tecnico-scientifica delle indagini effettuate sull’Allegoria dei cinque sensi di Mattia e
699 Gregorio Preti
700 Rosi F, Burnstock A, Van den Berg KJ, Miliani C, Brunetti BG, Sgamellotti A (2009) A non-invasive XRF study
701 supported by multivariate statistical analysis and reflectance FTIR to assess the composition of modern
702 painting materials. *Spectrochim Acta Part A Mol Biomol Spectrosc* 71:1655–1662.
703 <https://doi.org/10.1016/j.saa.2008.06.011>
704 Ruffolo SA, La Russa MF, Barca D, Casoli A, Comite V, Nava G, Crisci GM, De Francesco AM, Miriello D
705 (2010) Mineralogical, petrographic and chemical analyses for the study of the canvas “Cristo alla Colonna”
706 from Cosenza, Italy: A case study. *Period di Mineral* 79:71–79. <https://doi.org/10.2451/2010PM0022>
707 Tschegg C, Ntaflos T, Hein I (2009) Integrated geological, petrologic and geochemical approach to establish
708 source material and technology of Late Cypriot Bronze Age Plain White ware ceramics. *J Archaeol Sci*
709 36:1103–1114. <https://doi.org/10.1016/j.jas.2008.12.004>
710 Vahur S, Teearu A, Peets P, Joosu L, Leito I (2016) ATR-FT-IR spectral collection of conservation materials in
711 the extended region of 4000-80 cm⁻¹. *Anal Bioanal Chem* 408:3373–3379. [https://doi.org/10.1007/s00216-](https://doi.org/10.1007/s00216-016-9411-5)
712 016-9411-5
713 Venuti V, Fazzari B, Crupi V, Majolino D, Paladini G, Morabito G, Certo G, Lamberto S, Giacobbe L (2020) In
714 situ diagnostic analysis of the XVIII century Madonna della Lettera panel painting (Messina, Italy).
715 *Spectrochim Acta Part A Mol Biomol Spectrosc* 228:117822. <https://doi.org/10.1016/j.saa.2019.117822>
716 Yilmaz HM, Yakar M, Gulec SA, Dulgerler ON (2007) Importance of digital close-range photogrammetry in
717 documentation of cultural heritage. *J Cult Herit* 8:428–433. <https://doi.org/10.1016/j.culher.2007.07.004>
718 Zuena M, Buemi LP, Stringari L, Legnaioli S, Lorenzetti G, Palleschi V, Nodari L, Tomasin P (2020) An
719 integrated diagnostic approach to Max Ernst’s painting materials in his Attirement of the Bride. *J Cult Herit*
720 43:329–337. <https://doi.org/10.1016/j.culher.2019.10.010>
721